Video Article

Assessing Tumor Microenvironment of Metastasis Doorway-Mediated Vascular Permeability Associated with Cancer Cell Dissemination using Intravital Imaging and Fixed Tissue Analysis

George S. Karagiannis[1,2,3], Jessica M. Pastoriza[1,2,4], Lucia Borriello[1,2], Rojin Jafari[1,2], Anouchka Coste[1,2,4], John S. Condeelis[1,2,3,4], Maja H. Oktay[1,2,3,5], David Entenberg[1,2,3]

[1]Department of Anatomy and Structural Biology, Albert Einstein College of Medicine

[2]Gruss-Lipper Biophotonics Center, Albert Einstein College of Medicine

[3]Integrated Imaging Program, Albert Einstein College of Medicine

[4]Department of Surgery, Montefiore Medical Center

[5]Department of Pathology, Montefiore Medical Center

Correspondence to: George S. Karagiannis at georgios.karagiannis@einstein.yu.edu, John S. Condeelis at john.condeelis@einstein.yu.edu, Maja H. Oktay at maja.oktay@einstein.yu.edu, David Entenberg at david.entenberg@einstein.yu.edu

URL: https://www.jove.com/video/59633
DOI: doi:10.3791/59633

Keywords: Cancer Research, Issue 148, intravital imaging, immunofluorescence, blood vessel permeability, tumor microenvironment of metastasis (TMEM), high molecular weight dextran, immunofluorescence, metastasis

Date Published: 6/26/2019

Citation: Karagiannis, G.S., Pastoriza, J.M., Borriello, L., Jafari, R., Coste, A., Condeelis, J.S., Oktay, M.H., Entenberg, D. Assessing Tumor Microenvironment of Metastasis Doorway-Mediated Vascular Permeability Associated with Cancer Cell Dissemination using Intravital Imaging and Fixed Tissue Analysis. *J. Vis. Exp.* (148), e59633, doi:10.3791/59633 (2019).

Abstract

The most common cause of cancer related mortality is metastasis, a process that requires dissemination of cancer cells from the primary tumor to secondary sites. Recently, we established that cancer cell dissemination in primary breast cancer and at metastatic sites in the lung occurs only at doorways called Tumor MicroEnvironment of Metastasis (TMEM). TMEM doorway number is prognostic for distant recurrence of metastatic disease in breast cancer patients. TMEM doorways are composed of a cancer cell which over-expresses the actin regulatory protein Mena in direct contact with a perivascular, proangiogenic macrophage which expresses high levels of TIE2 and VEGF, where both of these cells are tightly bound to a blood vessel endothelial cell. Cancer cells can intravasate through TMEM doorways due to transient vascular permeability orchestrated by the joint activity of the TMEM-associated macrophage and the TMEM-associated Mena-expressing cancer cell. In this manuscript, we describe two methods for assessment of TMEM-mediated transient vascular permeability: intravital imaging and fixed tissue immunofluorescence. Although both methods have their advantages and disadvantages, combining the two may provide the most complete analyses of TMEM-mediated vascular permeability as well as microenvironmental prerequisites for TMEM function. Since the metastatic process in breast cancer, and possibly other types of cancer, involves cancer cell dissemination via TMEM doorways, it is essential to employ well established methods for the analysis of the TMEM doorway activity. The two methods described here provide a comprehensive approach to the analysis of TMEM doorway activity, either in naïve or pharmacologically treated animals, which is of paramount importance for pre-clinical trials of agents that prevent cancer cell dissemination via TMEM.

Video Link

The video component of this article can be found at https://www.jove.com/video/59633/

Introduction

Recent advances in our understanding of cancer metastasis have uncovered that epithelial-to-mesenchymal transition (EMT) and the induction of a migratory/invasive cancer cell subpopulation are not, by themselves, sufficient for hematogenous dissemination[1]. Indeed, it was previously thought that metastasizing cancer cells intravasate through the entirety of cancer-associated endothelium as the tumor neovasculature is often characterized by low pericyte coverage, and as such, is highly permeable and unstable[2,3,4]. Although highly suggestive of defective functions within the tumor, vascular modifications during carcinogenesis do not provide evidence per se that tumor cells can penetrate blood vessels easily and in an uncontrolled fashion. Insights from intravital imaging (IVI) studies, in which tumor cells are fluorescently-tagged and the vasculature is labeled via the intravenous injection of fluorescent probes (such as dextran or quantum dots), show that, while tumor vessels are uniformly permeable to low molecular weight dextrans (e.g. 70 kD), high molecular weight dextrans (155 kD) and tumor cells can cross the endothelium only at specialized sites of intravasation which are preferentially located at vascular branch point[5,6,7]. Immunohistochemical (IHC) analyses using animal models and human patient-derived material have shown that these sites are "doorways" that specialize in regulating vascular permeability, locally and transiently, providing a brief window of opportunity for migratory/invasive cancer cells to enter the circulation. These doorways are called "Tumor Microenvironment of Metastasis" or "TMEM", and, quite expectedly, their density correlates with an increased risk of developing metastatic disease in breast cancer patients[8,9,10].

Each TMEM doorway consists of three distinct types of cells: a perivascular macrophage, a tumor cell over-expressing the actin-regulatory protein mammalian enabled (Mena), and an endothelial cell, all in direct physical contact with each other[1,5,9,10,11,12,13]. The key event for the function of TMEM as an intravasation doorway is the localized release of vascular endothelial growth factor (VEGF) onto the underlying vessel by the perivascular macrophage[14]. VEGF can disrupt homotypic junctions between endothelial cells[15,16,17,18,19], a phenomenon that results in transient vascular leakage, also known as "bursting" permeability as described in IVI studies [5]. TMEM macrophages have been shown to express the tyrosine kinase receptor TIE2, which is required for VEGF-mediated TMEM function and homing of these macrophages to the perivascular niche[5,20,21,22]. In addition to regulating cancer cell dissemination and metastasis, $TIE2^+$ macrophages have been shown to be central regulators of tumor angiogenesis[21,22,23,24,25,26,27,28,29,30,31]. As such, $TIE2^+$ macrophages represent a critical constituent of the tumor microenvironment and the main regulator of the metastatic cascade.

To better conceptualize TMEM-mediated vascular permeability (i.e. "bursting"), it is very important to distinguish it from other modes of vascular permeability that are not associated with the dissolution of endothelial cell-cell junctions. In an intact endothelium (one whose tight and adherens junctions are not disrupted), there are three main types of vascular permeability: (a) pinocytosis, which may, or may not, be coupled to transcytosis of the ingested material; (b) transportation of material through endothelial fenestrae; and (c) transportation of material through the paracellular pathway, which is regulated by endothelial tight junctions[15,16,17,18,19,32,33,34]. Although deregulated in many tumors, the aforementioned modes of vascular permeability have been described mostly in the context of normal tissue physiology and homeostasis, the extremes of which are tissues with either limited permeability (e.g., blood-brain barrier, blood-testis barrier), or abundant permeability (e.g., fenestrated capillaries of the kidney glomerular apparatus)[34,35,36,37].

Using multiphoton intravital imaging and multiplexed immunofluorescence microscopy, we are able to distinguish between TMEM-mediated vascular permeability ("bursting") and other modes of vascular permeability in breast tumors. To achieve this, we perform a single intravenous injection of a high-molecular weight, fluorescently-labeled probe in mice. Spontaneous bursting events can then be captured using intravital imaging in live mice; or alternatively, extravasation of the probe can be quantified by co-localization studies with blood vasculature (e.g. $CD31^+$ or $Endomucin^+$) and TMEM doorways using immunofluorescence microscopy. The protocols presented here describe both of these techniques, which could be used either independently or in conjunction with one another.

Protocol

All experiments using live animals must be conducted in accordance with animal use and care guidelines and regulations. The procedures described in this study were carried out in accordance with the National Institutes of Health regulations concerning the care and use of experimental animals and with the approval of the Albert Einstein College of Medicine Animal Care and Use Committee (IACUC).

1. Evaluation of "bursting permeability" using live animal imaging

1. **Transplantation of syngeneic breast tumors into mouse hosts with fluorescent macrophages**
    1. Generate pieces of tumor tissue suitable for transplantation.
        1. Generate fluorescently-labeled tumors in mouse mammary cancer models by crossing the spontaneous, autochthonous, genetically engineered mouse mammary cancer model MMTV-PyMT mice with transgenic mice expressing fluorescent reporters[38,39] [e.g., enhanced green fluorescent protein (EGFP), enhanced cyan fluorescent protein (ECFP), or Dendra2].
        2. Allow the MMTV-PyMT mice with fluorescently labeled tumors to grow to a size of no larger than 2 cm (approximately 10-12 weeks of age).
        3. Euthanize the tumor bearing MMTV-PyMT mice by placing them into a chamber with 5% isoflurane until 30 seconds after all respirations stop.
        4. Perform a cervical dislocation.
        5. Remove hair from the euthanized mouse's abdomen using a topical depilatory cream.
        6. Place a Petri dish with DMEM/F12 cell culture medium on ice.
        7. Place the mouse and Petri dish on ice into the fume hood.
        8. Sanitize the mouse's abdomen with 70% ethyl alcohol.
        9. Using sterile gloves and surgical tools (sterilized scissors, forceps, and blade) remove the tumors and place them into the Petri dish.
        10. Cut up the tumor into small pieces (~2 mm x 2 mm x 2mm in size), discarding any necrotic portions, while they are in the Petri dish.
    2. Transplant the tumor pieces into recipient hosts.
        1. Raise mice with genetically engineered fluorescently-labeled macrophages, e.g., MacGreen[40] or MacBlue [41] mice (*Csf1r*-GAL4VP16/UAS-ECFP)
        2. Allow the FVB mice with fluorescently labeled macrophages to grow to an age of ~4-6 weeks).
        3. Anesthetize the FVB mice with fluorescently labeled macrophages in a chamber using 5% isoflurane with oxygen as a carrier gas.
        4. Reduce the anesthesia to ~3% isoflurane and apply ophthalmic ointment to the eyes of the mouse to prevent drying.
        5. Remove hair from over the 4^{th} mammary gland of the mouse.
        6. Clean the skin with betadine. It is important to maintain sterile conditions throughout the rest of the procedure. This includes using sterilized instruments and reagents.
        7. Make a small incision ~2-3 mm just inferior to the 4^{th} nipple.
        8. Dissect until the mammary fat pad is exposed.
        9. Take a tumor piece from the Petri dish and coat in artificial extracellular matrix.
        10. Transplant tumors underneath the 4^{th} mammary fat pad.
        11. Close the incision using cyanoacrylate adhesive.

12. Continuously monitor the animal until it fully recovers from anesthesia and is able to maintain sternal recumbency. Also, do not to return the animal to the company of other animals until full recovery.
13. To minimize infections, add 1 mL of 100 mg/mL enrofloxacin antibiotic to the animal's drinking water bottle (8 fl oz).
14. Allow tumors to grow until palpable (~5 mm; ~4 weeks).
15. Depending on the experiment, allocate the mice into treatment groups, and perform the corresponding treatments, if applicable.

2. **Setup for intravital imaging**
   1. Turn on microscope's two-photon laser and detectors.
   2. Turn on the heating box and pre-heat the microscope's x-y stage.
   3. Place the custom-made stage insert[42] into the x-y stage.

3. **Preparation of imaging window**
   1. Prior to setting up for imaging, autoclave the custom-made circular imaging window frame[42].
   2. Use a pipette or an insulin syringe to place a thin layer of cyanoacrylate adhesive to the window frame and affix in place an 8 mm circular cover glass.
      NOTE: 1) It is important to avoid getting residue on the clear aperture of the cover glass. 2) It is important to adhere the cover glass to the window frame at least 1 h before use for imaging.
   3. Carefully wipe clean any excess cyanoacrylate on the clear aperture of the cover glass using a laboratory wipe wetted with a small amount of acetone.

4. **Preparation of tail vein catheter for administration of fluids and fluorescent dyes during imaging**
   1. Cut a 30 cm piece of polyethylene tubing to construct a tail vein catheter.
   2. Detach the needle portion of a 30 G needle from its Luer taper by gently bending the needle back and forth until it breaks.
      NOTE: The needle should be held close to the Luer taper and not the needle tip. This can be performed with pliers or forceps to grasp the needle in order to prevent needle stick injury.
   3. Insert the blunt end of the needle into one end of the polyethylene tubing.
   4. Insert the sharp end of another 30 G needle, keeping its Luer taper attached, to the opposite end of the tubing.
   5. Fill a 1 cc syringe with phosphate buffered saline, attach it to Luer taper of the assembled catheter, and flush the tail vein catheter making sure that there are no air bubbles in the system.
   6. For vascular labeling, fill a 1 cc syringe with 100 µL of 10 mg/kg 155 kDa dextran-tetramethylrhodamine (TMR) or quantum dots.

5. **Preparation of mouse for imaging**
   1. Anesthetize the mouse in a cage underneath (~1 foot below) a heat lamp using 4%-5% isoflurane mixed with 100% oxygen set to a flow of 1.5-2 L per min.
   2. Turn on heat lamp over surgical working area. This step is critical for maintaining the core physiologic body temperature of the mouse during the surgery.
   3. Place the mouse under the heat lamp and lower the anesthesia to 2%-3% for the duration of the surgery.
      NOTE: Be sure to keep the heat lamp at a safe distance (~1 foot) away from the mouse to avoid overheating.
   4. Place ophthalmic ointment on the mouse's eyes to prevent drying of the eyes and blindness.
   5. Test that the mouse is anesthetized by performing toe-pinch test. If animal withdraws, increase dosage of isoflurane by 1% and retest in 1-2 min.
   6. Insert the tail vein catheter into the most distal point on the tail possible.
   7. Affix the tail vein catheter to the tail with a small piece of lab tape that wraps around the tail and sticks to the needle to insure it does not get dislodged.
   8. Inject 50 µL per h of PBS through the tail vein catheter to provide adequate hydration. It is critical to avoid injecting too much fluid (no more than 200 µL per h) or any bubbles into the catheter as this can be fatal to the mouse.
   9. Remove hair on the abdomen over the 4^{th} and 5^{th} mammary glands using depilatory cream.
   10. Clean the skin with betadine and allow skin to dry.
   11. Make a longitudinal midline incision starting immediately superior to the genitals and carry the incision up to the level of the superior aspect of the 4^{th} mammary gland.
   12. Carry the incision transverse to the superior aspect of the 4^{th} mammary gland. It is critical to avoid compromising the blood supply at this point.
   13. Dissect the mammary fat pad off the peritoneum creating a tissue flap using sterile forceps and scissors.
       NOTE: Skin flap imaging is susceptible to significant motion artifacts and tissue dehydration. These are avoided, as described previously[43,44], by affixing a rigid piece of rubber behind to the skin side of the flap (to stiffen the soft tissue and isolate it from the rest of the body) and then placing the tumor into a shallow imaging window to preserve the hydration. This is critical for stable imaging as the tumor and surrounding tissue in this setting are very compliant.
   14. Stabilize the skin flap by affixing (with cyanoacrylate glue) a small piece of rigid rubber measuring 2 cm x 2 cm to the skin side of the flap. The tumor should be in the center of the area being stabilized by the rubber.
   15. Keep exposed tissue hydrated with drops of PBS.
   16. Apply a small film of cyanoacrylate to the outer rim of the custom-made imaging window frame.
   17. Apply a small droplet of PBS (~10–20 µL) to the center of the cover glass.
   18. Dry the surrounding flap tissue with a laboratory wipe. It is critical to make sure that the cyanoacrylate on the window frame does not come into contact with the PBS on the glass, as this can cause the cyanoacrylate to polymerize and set prematurely.
   19. Affix the small imaging window to the tissue flap with the tumor at the center of the clear aperture.
   20. Remove the heating box from the stage.
   21. Transfer the anesthetized mouse and tail vein catheter to the microscope stage. Use extreme caution to ensure the tail vein catheter does not fall out.
   22. Place mouse on the stage in the prone position.

23. Place the nose cone of isoflurane over the snout to ensure maintenance of anesthesia.
24. Insert the window into the bore on the custom x-y stage plate.
25. Place the heating box back onto the stage to maintain a physiological temperature.
26. Monitor the animal's vital signs by attaching a pulse oximeter probe via clip sensor to the back paw.
27. Slowly decrease isoflurane to 0.5%-1% to maintain adequate blood flow and avoid over anesthetizing the mouse.

6. **Intravital imaging**
NOTE: The imaging we describe in this section was performed on a custom-built two-laser multiphoton microscope that has been previously described[5,39,45]. Briefly, a femtosecond laser is used to generate 90 femtosecond pulsed laser light centered at 880 nm. Fluorescence light is detected with three of the four simultaneously acquiring detectors (Blue = 447/60, Green = 520/65, and Red 580/60; central wavelength/ bandwidth) after separation from the excitation light by a dichroic (Chroma, Z720DCXXR). The microscope stand contains a 25x, 1.05 NA (numerical aperture) long working distance (2 mm) objective lens. It is important to note that, while we have used a custom-built microscope, the protocol described below can be accomplished on any commercially available multiphoton microscope as well.
    1. Place a drop of distilled water between the 25x, 1.05 NA microscope objective and the window's cover glass to make optical contact.
    2. Use the microscope eyepiece to focus on areas with fluorescent tumor cells near to the surface of the window.
    3. Find flowing blood vessels and labeled macrophages. It is critical to have flowing blood vessels to assess the dynamics of the vasculature.
    4. Switch the microscope into multiphoton mode.
    5. Set the upper and lower limits of a z-series, which measures approximately 50 µm.
        1. Set the upper limit of the z-series by using the focus adjuster to move the objective to the desired start location, at the most superficial position, and marking this position as zero within the software by clicking on the Z position **Top** button.
        2. Set the lower limit of the z-series moving the objective to the deepest layer (typically 50-70 µm from the top for smaller tumors) and clicking the Z position **Bottom** button.
        3. Set the z-step size to 5 µm.
    6. Click the Time-Lapse panel button and set the time interval between acquisitions to at least 10 s to provide adequate time to replenish the water above the objective lens. This is done manually with a squeeze pipette on the objective during the long time lapse.
    7. Remove the syringe with PBS in the tail vein catheter and replace it with another syringe containing the 155 kDa dextran-TMR (tetramethyl rhodamine).
    8. Inject 100 µL of 155 kDa dextran-TMR via the tail vein catheter.
    9. After injection, replace the TMR syringe with the PBS syringe.
    10. Acquire a z-stack time-lapse imaging by clicking on the Z-Stack and Time-Lapse buttons, then clicking on the record button.
    11. Inject 50 µL of PBS every 30-45 min to maintain adequate hydration of the animal. Avoid injecting more than 200 µL at time as this can cause fluid overload.

7. **Euthanasia**
    1. Increase the isoflurane to 5% and keep the animal under 5% isoflurane with nose cone in place until 30 s after respirations cease.
    2. Remove the mouse from the stage.
    3. Perform cervical dislocation.

8. **Image processing**
    1. Load all images into ImageJ and format them into a 5 dimensional hyperstack (x, y, z, t, and color channel).
    2. Perform separation of spectral overlap (i.e.: GFP and CFP) and elimination of x-y drift from the hyperstacks using established methods[38].
    3. Use the brightness and contrast adjustment to increase the white level of the blood channel so that the background signal becomes visible.
    4. For each z slice, carefully inspect each movie for signs of transient vascular leakage (a "burst"). Running the movies at fast frame rates (40 fps) may aid this identification.
    5. Once a burst has been identified, return the brightness for this channel to a normal level and crop the hyperstack to this region and z-slice.

2. Evaluation of extravascular dextran using fixed tissue analysis

1. **Tumor and sample preparation**
NOTE: The 2nd part of this protocol assumes that breast tumors have been harvested from an orthotopic transplantation mouse model of breast carcinoma (i.e. the MMTV-PyMT). This model could be the same as the one described in the 1st part of the protocol, although fluorescently-labeled tumors are not necessary at this point.
    1. Following the termination of the experimental pipeline (i.e. drug treatments, etc.), perform a tail-vain injection of 100 µL of 10 mg/mL 155 kDa dextran-tetramethyl rhodamine, 1 h before sacrificing the mice.
    2. Sacrifice the mice and harvest the breast tumors.
    3. Fix tumors in 10% formalin for 48-72 h and proceed to paraffin-embedding.
    4. Using a microtome, cut two 5 µm-thick sequential slides from the formalin-fixed paraffin-embedded (FFPE) tissues. One slide is used for staining the dextran, while the other will be used for performing TMEM triple-IHC, for reference.
    NOTE: The TMEM triple-immunohistochemistry protocol has been described elsewhere [10].

2. **IF staining and scanning for the first of the two sequential sections**
    1. Submit slides to a standard de-paraffinization protocol. This includes two subsequent immersions in xylene (10 min each), followed by dehydration in serially diluted alcohol solutions (100%, 95%, 70%, and 50% EtOH in H_2O for 2 min each immersion).
    2. Perform antigen retrieval by heating (close to boiling point) the sections submerged in citrate (pH 6.0-adjusted) for 20 min.

3. Let the samples cool to room temperature for 15-20 min and then wash in PBS 3x for 2 min each wash.
4. Block for 60-90 min in blocking buffer (10% FBS; 1% BSA; 0.0025% fish skin gelatin; 0.05% PBST, i.e. PBS with 0.05% Tween-20).
5. Incubate samples with a mixture of primary rat and rabbit antibodies which target Endomucin and TMR, respectively, and then wash in PBST 3x, 2 min each.
6. Incubate samples with a mixture of secondary donkey antibodies against rat IgG (conjugated to Alexa-647) and rabbit IgG (conjugated to Alexa-488), and then wash in PBST 3x 2 min each.
7. Perform a routine DAPI staining (i.e. immersion in DAPI solution for 5-6 min), mount the slides using a glycerol-free "hard" mounting medium, and store in a dark place until scanning.
8. For optimal results, scan the slides on a digital whole slide scanner.

3. **Image Analysis**
   1. Capture 10 High Power Fields (HPFs) per case, using any software suitable for digital pathology.
   2. Save the Endomucin (Red) and TMR (Green) channels separately as TIFF.
   3. Using ImageJ, upload the TIFF files and convert them into 8-bit images.
   4. Threshold the 8-bit images to the level of the negative control, and generate two binarized images, showing the Endomucin and TMR "masks".
   5. From the **Binary** tools, select **Fill Holes** on the Endomucin mask.
      1. Generate and save the following five regions of interest: 1) The thresholded dextran image as "Dextran ROI" (ROI1), 2) the thresholded endomucin image as "Vascular ROI" (ROI2), 3) the inverted endomucin image as "Extravascular ROI" (ROI3), 4) the intersected "Extravascular ROI" and "Dextran ROI" image (ROI1 ∩ ROI3) as "Extravascular Dextran ROI" (ROI4), and 5) the entire image as "Tumor ROI" (ROI5).
   6. Divide the ROI4 area by the ROI5 area and multiply by 100 to generate the percent area that the extravascular dextran covers in the entire tumor.
   7. Repeat the process for 10-20 HPFs per case (depending on tissue availability) and generate an average Extravascular Dextran (% area) for each case.

Representative Results

The experimental procedures described in this protocol article are briefly summarized and illustrated in **Figure 1A-C**.

To measure TMEM-mediated vascular permeability ("bursting activity") and to reduce experimental noise from other modes of vascular permeability (i.e. transcellular and paracellular, as explained in the introduction), we performed intravenous (i.v.) injection of high molecular weight probes, such as 155 kDa Dextran, conjugated to tetramethyl rhodamine. Lower molecular weight dextrans did not distinguish the three modes of vascular permeability. Our prior experience has indicated that the systemic circulation of 155 kDa TMR-Dextran efficiently labeled the vasculature of both normal tissues, such as the mammary gland and the lungs (**Figure 2A,B**), as well as of neoplastic tissues, such as primary breast cancer and breast cancer metastases in lungs (**Figure 2C,D**). As also confirmed by prior studies[5,46], 155 kDa TMR-Dextran is thus a suitable probe for measuring “bursting” in both primary and secondary tumor sites. A characteristic example of peak bursting activity (dotted yellow area), using multiphoton intravital imaging in a primary MMTV-PYMT breast tumor is illustrated as a series of still images (**Figure 3A**). Bursting activity was always noted in association with a TMEM doorway (dotted white circle), characterized by the spatial juxtaposition of a Dendra2^{+} tumor cell a CFP^{+} macrophage and endothelium (**Figure 3A**). As mentioned, each TMEM doorway consists of a perivascular macrophage, a Mena overexpressing tumor cell, and an endothelial cell, all in direct physical contact with each other. While Mena has not been explicitly labeled in the mouse models used in these experiments, it has previously been shown to become overexpressed in late stage PyMT carcinoma[47]. This simplifies the identification of TMEM doorways and eliminates the need to explicitly label Mena in the tumor cells.

To assess TMEM-dependent vascular permeability in fixed tissue analysis, we performed the procedure described in this protocol in mice which were transplanted with tumor chunks taken from 14-week old MMTV-PyMT donor mice. When mice reached an appropriate tumor size, they received a single i.v. dose of 155-kDa TMR-Dextran, as described in Part 2 of this protocol, and were sacrificed after 1 hour. The tumor tissues were collected and subjected to IF analysis. The endomucin fluorescent signal was used as an exclusion mask to the dextran fluorescent signal, allowing for discrimination between highly-permeable and low, or non-permeable, blood vessels (**Figure 3B**). As previously described in Karagiannis et al.[48], a sequential slide was also stained with the previously-established TMEM triple stain and aligned with the corresponding IF slide. Using this approach, we confirmed that the highly-permeable blood vessels within the breast tumor tissue have at least one associated TMEM doorway (**Figure 3B**).

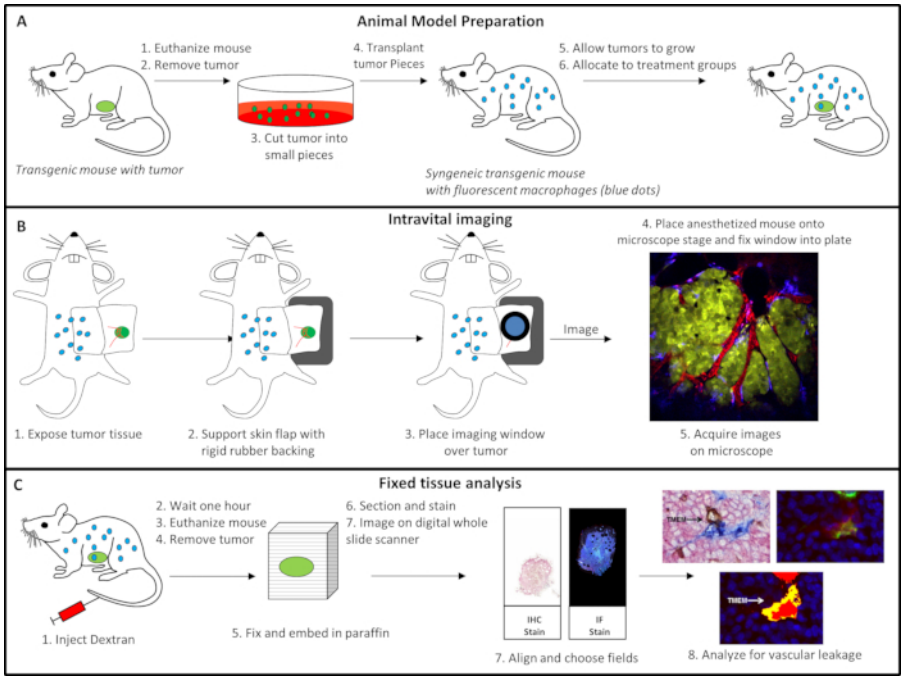

Figure 1. Summary of procedure. (**A**) Dendra-2 labeled invasive carcinoma of the breast (green) taken from a transgenic animal [*FVB/N-Tg(MMTV-PyMT)mul-Tg(MMTV-iCre)Jwp-Tg(loxP-stop-loxP-Pdendra2)Jwp*] and cut into small pieces. One piece is then orthotopically transplanted into another transgenic animal whose macrophages were labeled by cyan fluorescent protein (cyan) [*FVB/N-Tg(Cfms-gal4-vp16)-(UAS-eCFP)*]. The orthotopically transplanted to tumor is then allowed to grow, after which the mouse is allocated to the appropriate treatment arm. (**B**) Once the treatment is finished, the mouse is then taken for intravital imaging. Once anesthetized, a skin flap surgery is performed then stabilized with a rubber backing. A shallow imaging window is then affixed over the tumor. Finally, the mouse is then placed on the microscope stage where the window fits into the custom-made stage plate and the images can then be acquired. (**C**) Alternatively, the mouse from **A** is administered high molecular weight dextran and sacrificed after 1 hour. The tumor is then removed, fixed, and processed for paraffin embedding. Sections of the tissue are cut, stained for TMEM in IHC and dextran and vessels in IF, and scanned on a digital whole slide scanner. Finally, images from the two scans are aligned and individual fields of view are chosen for analysis and quantification of vascular leakage. Please click here to view a larger version of this figure.

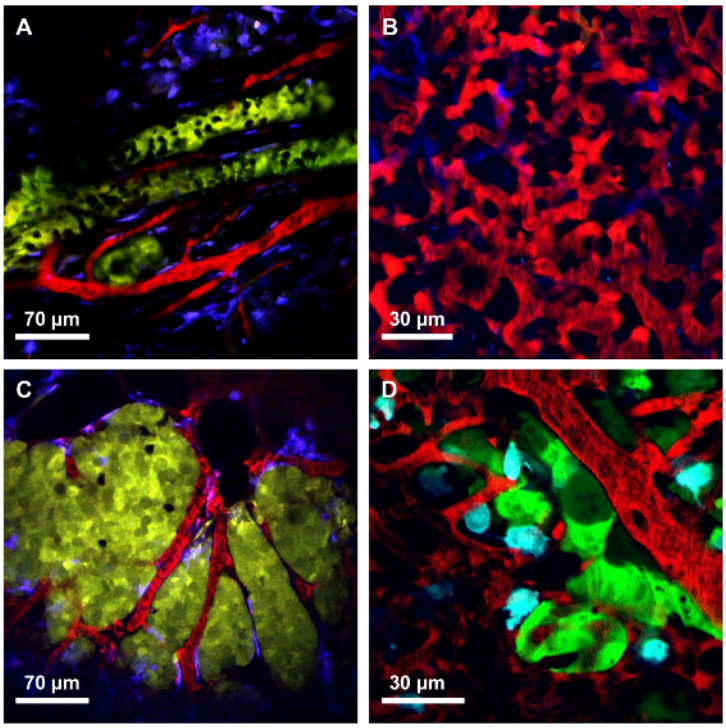

Figure 2. Visualization of TMR-Dextran labeled vasculature in healthy and diseased tissues. (**A**) Image of a healthy developing mammary gland within a transgenic animal whose vasculature is labeled by TMR-Dextran (red), mammary ductal epithelium labeled by the fluorescent protein Dendra-2 (green), and macrophages labeled by a cyan fluorescent protein (blue) [*FVB/N-Tg(loxP-stop-loxP-Pdendra2)Jwp-Tg(Cfms-gal4-vp16)-(UAS-eCFP)*]. (**B**) Healthy lung tissue visualized through a lung imaging window within a mouse whose vasculature is labeled by TMR-Dextran (red). Blue = SHG from collagen fibers. (**C**) Dendra2 labeled invasive ductal carcinoma taken from a transgenic animal [*FVB/N-Tg(MMTV-PyMT)mulxTg(MMTV-iCre)Jwp-Tg(loxP-stop-loxP-Pdendra2)Jwp*] and orthotopically transplanted into another transgenic animal whose macrophages are labeled by cyan fluorescent protein (blue) [*FVB/N-Tg(Cfms-gal4-vp16)-(UAS-eCFP)* and vessels labeled with TMR-Dextran (red). (**D**) Lung metastases eight days after iv injection of tumor cells (E0771; labeled by the fluorescent protein Clover) into a transgenic animal whose macrophages are labeled by cyan fluorescent protein (cyan) [*FVB/N-Tg(Cfms-gal4-vp16)-(UAS-eCFP)]* and vasculature labeled by TMR-Dextran (red). Please click here to view a larger version of this figure.

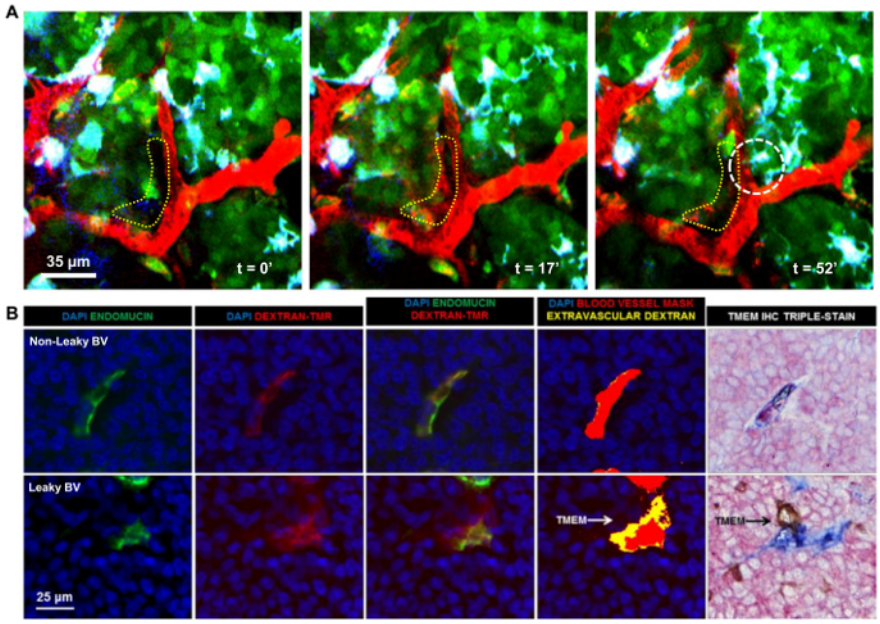

Figure 3. Visualization of TMEM-mediated vascular permeability using intravital imaging and fixed tissue analysis. (**A**) Stills from a time-lapsed intravital imaging movie of 155-kDa TMR-Dextran labeling of neo-angiogenic vessels (red) within a Dendra-2 labeled invasive carcinoma of the breast (green) taken from a transgenic animal [*FVB/N-Tg(MMTV-PyMT)mul-Tg(MMTV-iCre)Jwp-Tg(loxP-stop-loxP-Pdendra2)Jwp*] and orthotopically transplanted into another transgenic animal where the macrophages were labeled by cyan fluorescent protein (cyan) [*FVB/N-Tg(Cfms-gal4-vp16)-(UAS-eCFP)*]. The dotted yellow line denotes the outline of the transient vascular leakage area before (t = 0'), during (t = 17') and after (t = 52') the leakage (bursting) event. The dashed white circle points to a TMEM doorway, as captured in live imaging. (**B**) Multichannel immunofluorescence of Endomucin (first column), 155-kDa dextran-TMR (second column), their merged image along with DAPI (third column), the thresholded blood vessel and extravascular dextran masks (fourth column), and the corresponding sequential section of TMEM IHC (fifth column) in MMTV-PyMT mice. Top row: Vascular profile away from TMEM, appearing as a "non-leaky" vascular profile. Bottom row: TMEM-associated vascular profile, appearing as a "leaky" vascular profile. Please click here to view a larger version of this figure.

Discussion

Here, we outline two protocols that can be applied to visualize and quantify a specific type of vascular permeability which is present at TMEM doorways and is associated with the disruption of vascular tight and adherens junctions. This type of vascular permeability is transient and controlled by the tripartite TMEM cell complex, as explained above[5]. The ability to identify and quantify TMEM-associated vascular permeability is crucial for the assessment of a pro-metastatic cancer cell microenvironment, as well as for pre-clinical studies that examine the effect of conventional cytotoxic therapies on tumor microenvironment as well as anti-metastatic potential of targeted and non-targeted therapies. Importantly, we demonstrated here that this assessment can be done by either intravital imaging or immunofluorescence in fixed tissues. Both approaches have their advantages and disadvantages. Intravital imaging allows direct visualization of the dynamic process of vascular permeability, but requires specialized equipment and training. On the other hand, immunofluorescence performed in fixed tissues offers only a static image, but can be routinely performed in most laboratories.

Cancer patients are commonly treated with some form of systemic therapy, and the success of systemic treatment is usually assessed by the evaluation of parameters related to cancer cell survival such as apoptosis, proliferation, or gross tumor size. However, it is equally important to understand how these systemic therapies affect cancer cell dissemination given that most cancer related mortality occurs due to metastasis, a process which involves both cancer cell proliferation as well as cancer cell dissemination[1]. For example, recent studies have demonstrated that chemotherapy can induce a significant increase in the density of TMEM doorways in mouse and human breast cancer[48,49]. Moreover, it was shown that chemotherapy induces TMEM activity and results in hematogenous dissemination of cancer cells, increased circulating cancer cells, and increased lung metastasis[48]. The chemotherapy-induced increase in TMEM activity can be blocked by systemic administration of drug that inhibits TIE2 function and therefore TMEM activity, called rebastinib[14,48]. Thus, the protocols described here can offer valuable endpoint measurements for the effect of various systemic treatments on TMEM activity through the comparison of treated to non-treated cohorts of mice.

In recent years, the concept of antiangiogenic therapy in cancer has been revisited, suggesting that a vascular "normalization" strategy (i.e. the transient reconstitution of the abnormal structure and function of blood vessels), may be preferable to targeting blood vessels for destruction, as it makes the neovasculature more effective for drug delivery[50,51,52,53,54]. In view of this emerging hypothesis, other groups have also developed assays for assessing vascular permeability and for testing the efficiency of vascular normalization strategies[55]. It should be mentioned that, in principle, these methods are utilized to assess TMEM-independent modes of vascular permeability. Therefore, the selection of the most appropriate vascular permeability assay depends on the scope of a study, and researchers must ensure that they comprehend the applicability of each of the published vascular permeability assays, before applying them to their studies.

As mentioned above, each of the two methods described here has certain advantages over the other. For example, measuring "bursting permeability" in vivo offers valuable kinetic information, but since bursting is a rare event, prolonged imaging sessions of several hours each may be required to be able to obtain sufficient data. In addition, intravital imaging requires specialized equipment which may not available to all

investigators. On the other hand, evaluation of TMEM activity in fixed tissues is relatively easy to perform and requires only standard laboratory equipment. In addition, the analysis of TMEM activity in fixed tissues is easier to interpret, but lacks kinetic information. Moreover, the fixed tissue analysis is less specific, since it may capture cumulative leakage of dextran over time from transcellular and paracellular vascular permeability of intact endothelia, or even a sudden leakage event due to spontaneous vascular injury. Thus, the synergistic use of the two methods would make the interpretation of the TMEM-mediated vascular permeability more specific and more sensitive. While we have not explicitly tested other applications of the techniques presented here, they may prove useful for investigating induced vessel permeability, for example by infection or by pharmaceutical therapies.

In summary, the measurement of TMEM-associated vascular permeability, as outlined by two independent methodologies here, provide useful tools for assessing the pro-metastatic tumor microenvironment and its associated TMEM activity, and can be used to some extent by any laboratory. These methods are particularly useful in the pre-clinical assessment of the effect of systemic therapies on cancer cell dissemination. In addition, they can be used to assess the effect of agents that can block chemotherapy-induced TMEM activity, and lastly, these methods can be used to assess the best combination therapy preceding phase I patient trials.

Disclosures

The authors disclose no conflicts of interest.

Acknowledgments

We would like to thank the Analytical Imaging Facility (AIF) in the Albert Einstein College of Medicine for imaging support. This work was supported by grants from the NCI (P30CA013330, CA150344, CA 100324 and CA216248), the SIG 1S10OD019961-01, the Gruss-Lipper Biophotonics Center and its Integrated Imaging Program, and Montefiore's Ruth L. Kirschstein T32 Training Grant of Surgeons for the Study of the Tumor Microenvironment (CA200561).

GSK co-wrote the manuscript, performed imaging for figure 1C and 3B, developed fixed tissue analysis protocol, and analyzed and interpreted all data; **JMP** co-wrote the manuscript, and performed the surgery and intravital imaging for Figure 1B,2C and 3A; **LB & AC** performed the surgery and intravital imaging for Figure 2B; **RJ** performed the surgery and intravital imaging for Figure 2A; **JSC** co-wrote the manuscript and analyzed and interpreted all data; **MHO** co-wrote the manuscript and analyzed and interpreted all data; and **DE** performed the surgery and intravital imaging for Figure 2D, co-wrote the manuscript, developed fixed tissue analysis and intravital imaging protocols, and analyzed and interpreted all data.

References

1. Karagiannis, G. S., Goswami, S., Jones, J. G., Oktay, M. H., Condeelis, J. S. Signatures of breast cancer metastasis at a glance. *Journal of Cell Science.* **129** (9), 1751-1758, (2016).
2. Hanahan, D., Weinberg, R. A. Hallmarks of cancer: the next generation. *Cell.* **144** (5), 646-674, (2011).
3. Raza, A., Franklin, M. J., Dudek, A. Z. Pericytes and vessel maturation during tumor angiogenesis and metastasis. *American Journal of Hematology.* **85** (8), 593-598, (2010).
4. Pietras, K., Ostman, A. Hallmarks of cancer: interactions with the tumor stroma. *Experimental Cell Research.* **316** (8), 1324-1331, (2010).
5. Harney, A. S. et al. Real-Time Imaging Reveals Local, Transient Vascular Permeability, and Tumor Cell Intravasation Stimulated by TIE2hi Macrophage-Derived VEGFA. *Cancer Discovery.* **5** (9), 932-943, (2015).
6. Kedrin, D. et al. Intravital imaging of metastatic behavior through a mammary imaging window. *Nature Methods.* **5** (12), 1019-1021, (2008).
7. Wyckoff, J. B. et al. Direct visualization of macrophage-assisted tumor cell intravasation in mammary tumors. *Cancer Research.* **67** (6), 2649-2656, (2007).
8. Sparano, J. A. et al. A metastasis biomarker (MetaSite Breast Score) is associated with distant recurrence in hormone receptor-positive, HER2-negative early-stage breast cancer. *npj Breast Cancer.* **3**, 42, (2017).
9. Rohan, T. E. et al. Tumor microenvironment of metastasis and risk of distant metastasis of breast cancer. *Journal of the National Cancer Institute.* **106** (8), (2014).
10. Robinson, B. D. et al. Tumor microenvironment of metastasis in human breast carcinoma: a potential prognostic marker linked to hematogenous dissemination. *Clinical Cancer Research.* **15** (7), 2433-2441, (2009).
11. Pignatelli, J. et al. Invasive breast carcinoma cells from patients exhibit MenaINV- and macrophage-dependent transendothelial migration. *Science Signaling.* **7** (353), ra112, (2014).
12. Oktay, M. H., Jones, J. G. TMEM: a novel breast cancer dissemination marker for the assessment of metastatic risk. *Biomarkers in Medicine.* **9** (2), 81-84, (2015).
13. Roussos, E. T. et al. Mena invasive (Mena(INV)) and Mena11a isoforms play distinct roles in breast cancer cell cohesion and association with TMEM. *Clinical & Experimental Metastasis.* **28** (6), 515-527, (2011).
14. Harney, A. S. et al. The Selective Tie2 Inhibitor Rebastinib Blocks Recruitment and Function of Tie2(Hi) Macrophages in Breast Cancer and Pancreatic Neuroendocrine Tumors. *Molecular Cancer Therapeutics.* **16** (11), 2486-2501, (2017).
15. Bates, D. O., Lodwick, D., Williams, B. Vascular endothelial growth factor and microvascular permeability. *Microcirculation.* **6** (2), 83-96 (1999).
16. Lee, Y. C. The involvement of VEGF in endothelial permeability: a target for anti-inflammatory therapy. *Current Opinion in Investigational Drugs.* **6** (11), 1124-1130 (2005).
17. Roberts, W. G., Palade, G. E. Neovasculature induced by vascular endothelial growth factor is fenestrated. *Cancer Research.* **57** (4), 765-772 (1997).

18. Stan, R. V. et al. Immunoisolation and partial characterization of endothelial plasmalemmal vesicles (caveolae). *Molecular Biology of the Cell.* **8** (4), 595-605 (1997).
19. Roberts, W. G., Palade, G. E. Increased microvascular permeability and endothelial fenestration induced by vascular endothelial growth factor. *Journal of Cell Science.* **108 (Pt 6)**, 2369-2379 (1995).
20. Arwert, E. N. et al. A Unidirectional Transition from Migratory to Perivascular Macrophage Is Required for Tumor Cell Intravasation. *Cell Reports.* **23** (5), 1239-1248, (2018).
21. Kadioglu, E., De Palma, M. Cancer Metastasis: Perivascular Macrophages Under Watch. *Cancer Discovery.* **5** (9), 906-908, (2015).
22. Hughes, R. et al. Perivascular M2 Macrophages Stimulate Tumor Relapse after Chemotherapy. *Cancer Research.* **75** (17), 3479-3491, (2015).
23. Riabov, V. et al. Role of tumor associated macrophages in tumor angiogenesis and lymphangiogenesis. *Frontiers in Physiology.* **5**, 75, (2014).
24. Squadrito, M. L., De Palma, M. Macrophage regulation of tumor angiogenesis: implications for cancer therapy. *Molecular Aspects of Medicine.* **32** (2), 123-145, (2011).
25. Ferrara, N. Role of myeloid cells in vascular endothelial growth factor-independent tumor angiogenesis. *Current Opinion in Hematology.* **17** (3), 219-224, (2010).
26. Solinas, G., Germano, G., Mantovani, A., Allavena, P. Tumor-associated macrophages (TAM) as major players of the cancer-related inflammation. *Journal of Leukocyte Biology.* **86** (5), 1065-1073, (2009).
27. Venneri, M. A. et al. Identification of proangiogenic TIE2-expressing monocytes (TEMs) in human peripheral blood and cancer. *Blood.* **109** (12), 5276-5285, (2007).
28. Lewis, C. E., De Palma, M., Naldini, L. Tie2-expressing monocytes and tumor angiogenesis: regulation by hypoxia and angiopoietin-2. *Cancer Research.* **67** (18), 8429-8432, (2007).
29. Mazzieri, R. et al. Targeting the ANG2/TIE2 axis inhibits tumor growth and metastasis by impairing angiogenesis and disabling rebounds of proangiogenic myeloid cells. *Cancer Cell.* **19** (4), 512-526, (2011).
30. Lewis, C. E., Ferrara, N. Multiple effects of angiopoietin-2 blockade on tumors. *Cancer Cell.* **19** (4), 431-433, (2011).
31. Gabrusiewicz, K. et al. Anti-vascular endothelial growth factor therapy-induced glioma invasion is associated with accumulation of Tie2-expressing monocytes. *Oncotarget.* **5** (8), 2208-2220, (2014).
32. Karagiannis, G. S., Condeelis, J. S., Oktay, M. H. Chemotherapy-induced metastasis: mechanisms and translational opportunities. *Clinical & Experimental Metastasis.* (2018).
33. Senger, D. R. et al. Tumor cells secrete a vascular permeability factor that promotes accumulation of ascites fluid. *Science.* **219** (4587), 983-985 (1983).
34. Obermeier, B., Verma, A., Ransohoff, R. M. The blood-brain barrier. *Handbook of Clinical Neurology.* **133**, 39-59, (2016).
35. Satchell, S. C., Braet, F. Glomerular endothelial cell fenestrations: an integral component of the glomerular filtration barrier. *American Journal of Physiology: Renal Physiology.* **296** (5), F947-956, (2009).
36. Stan, R. V. Endothelial stomatal and fenestral diaphragms in normal vessels and angiogenesis. *Journal of Cellular and Molecular Medicine.* **11** (4), 621-643, (2007).
37. Mruk, D. D., Cheng, C. Y. The Mammalian Blood-Testis Barrier: Its Biology and Regulation. *Endocrine Reviews.* **36** (5), 564-591, (2015).
38. Entenberg, D. et al. Imaging Tumor Cell Movement in Vivo. *Current Protocols in Cell Biology.* **58**(1), 19.7.1-19.7.19 (2013).
39. Entenberg, D. et al. Setup and use of a two-laser multiphoton microscope for multichannel intravital fluorescence imaging. *Nature Protocols.* **6** (10), 1500-1520, (2011).
40. Sasmono, R. T. et al. A macrophage colony-stimulating factor receptor-green fluorescent protein transgene is expressed throughout the mononuclear phagocyte system of the mouse. *Blood.* **101** (3), 1155-1163, (2003).
41. Ovchinnikov, D. A. et al. Expression of Gal4-dependent transgenes in cells of the mononuclear phagocyte system labeled with enhanced cyan fluorescent protein using Csf1r-Gal4VP16/UAS-ECFP double-transgenic mice. *Journal of Leukocyte Biology.* **83** (2), 430-433, (2008).
42. Entenberg, D. et al. Time-lapsed, large-volume, high-resolution intravital imaging for tissue-wide analysis of single cell dynamics. *Methods.* **128**, 65-77, (2017).
43. Pastoriza, J. M. et al. Black race and distant recurrence after neoadjuvant or adjuvant chemotherapy in breast cancer. *Clinical & Experimental Metastasis.* (2018).
44. Williams, J. K. et al. Validation of a device for the active manipulation of the tumor microenvironment during intravital imaging. *Intravital.* **5** (2), e1182271, (2016).
45. Harney, A. S., Wang, Y., Condeelis, J. S., Entenberg, D. Extended Time-lapse Intravital Imaging of Real-time Multicellular Dynamics in the Tumor Microenvironment. *Journal of Visualized Experiments.* (112), e54042, (2016).
46. Entenberg, D. et al. A permanent window for the murine lung enables high-resolution imaging of cancer metastasis. *Nature Methods.* **15** (1), 73-80, (2018).
47. Roussos, E. T. et al. Mena invasive (MenaINV) promotes multicellular streaming motility and transendothelial migration in a mouse model of breast cancer. *Journal of Cell Science.* **124** (Pt 13), 2120-2131, (2011).
48. Karagiannis, G. S. et al. Neoadjuvant chemotherapy induces breast cancer metastasis through a TMEM-mediated mechanism. *Science Translational Medicine.* **9** (397), (2017).
49. Chang, Y. S., Jalgaonkar, S. P., Middleton, J. D., Hai, T. Stress-inducible gene Atf3 in the noncancer host cells contributes to chemotherapy-exacerbated breast cancer metastasis. *Proceedings of the National Academy of Sciences of the United States of America.* **114** (34), E7159-E7168, (2017).
50. Jain, R. K. Normalization of tumor vasculature: an emerging concept in antiangiogenic therapy. *Science.* **307** (5706), 58-62, (2005).
51. Winkler, F. et al. Kinetics of vascular normalization by VEGFR2 blockade governs brain tumor response to radiation: role of oxygenation, angiopoietin-1, and matrix metalloproteinases. *Cancer Cell.* **6** (6), 553-563, (2004).
52. Goel, S. et al. Normalization of the vasculature for treatment of cancer and other diseases. *Physiological Reviews.* **91** (3), 1071-1121, (2011).
53. Jain, R. K. Normalizing tumor microenvironment to treat cancer: bench to bedside to biomarkers. *Journal of Clinical Oncology.* **31** (17), 2205-2218, (2013).
54. Carmeliet, P., Jain, R. K. Principles and mechanisms of vessel normalization for cancer and other angiogenic diseases. *Nature Reviews Drug Discovery.* **10** (6), 417-427, (2011).

55. Meijer, E. F., Baish, J. W., Padera, T. P., Fukumura, D. Measuring Vascular Permeability In Vivo. *Methods in Molecular Biology.* **1458**, 71-85, (2016).